THE STRUCTURE OF TURBULENT AIR FLOW OVER WAVY WALL. PART2

Bandou, Toshiyuki
Department of Civil Engineering Hydraulics and Soil Mechanics, Kyushu University : Graduate student

Mitsuyasu, Hisashi
Research Institute for Applied Mechanics, Kyushu University : Professor

https://doi.org/10.5109/6781065

出版情報：Reports of Research Institute for Applied Mechanics. 35 (104), pp.13-34, 1988-09. 九州大学応用力学研究所
バージョン：
権利関係：

Reports of Research Institute for Applied Mechanics
Vol. XXXV, No. 104, 1988

THE STRUCTURE OF TURBULENT AIR FLOW OVER WAVY WALL. PART 2

By Toshiyuki BANDOU* and Hisashi MITSUYASU†

The structure of the turbulent shear flow over a solid wave surface is investigated experimentally for the sinusoidal wave with height-to-length ratio $H/L = 0.1$. Mean vertical profile of the wind velocity, which has been obtained by averaging the vertical profiles at different phases over one-wavelength, shows the logarithmic profile which is similar to those over the flat plate. The turbulent intensities $\overline{u'^2}$, $\overline{w'^2}$ and the turbulent Reynolds stress $-\overline{u'w'}$ for the wave surface agree with those for the flat plate at the same Reynolds number of $Re_{XP}(=U_0X_P/\nu) \fallingdotseq 6\times10^5$ if they are normalized with the friction velocity u_τ, where U_0 is the mean velocity of the free stream and X_P the distance from the leading edge of the test plates. The longitudinal distribution of the turbulent shear stress along the wave surface shows the occurence of the separation of the air flow at the wave crest. The momentum flux toward the wave surface is approximated by the turbulent Reynolds stress $-\overline{u'w'}$ in the logarithmic layer because the wave induced Reynolds stress $-\overline{\tilde{u}\tilde{w}}$ in this layer is negligible as compared to the turbulent Reynolds stress. However, the turbulent Reynolds stress in the logarithmic layer is roughly half of the stress $\overline{P\frac{\partial\eta}{\partial x}}+\overline{\sigma\frac{\partial\eta}{\partial x}}+\overline{\tau}$ measured at the wave surface, where P, σ and τ are the pressure, the turbulent normal stress and the turbulent tangential stress acting on the wave surface, respectively.

key words: turbulent flow over a wave surface, wind wave generation, wind-wave interaction, wave-induced velocity fluctuations, air flow separation, momentum transfer

* Graduate student, Department of Civil Engineering Hydraulics and Soil Mechanics, Kyushu University.
† Professor, Research Institute for Applied Mechanics, Kyushu University.

1. Introduction

This paper is a sequel to our previos paper Part 1 with the same title (Bandou et al. 1988)[1]. In Part 1, the pressure distribution along the solid wave surface under the action of the turbulent wind was measured for a sinusoidal wave and a Stokes wave with the height-to-length ratio $H/L = 0.1$. According to the previous study, the pressure distribution along each wave surface was described well by the first mode of the pressure distribution with the same wave number with that of the each wave surface. Although the amplitude of the first mode of the pressure distribution did not change much with the Reynolds number, the phase angle gradually increased with the decrease of the Reynolds number. This caused the increase of the form drag.

On the other hand, Zilker & Hanratty (1979)[2] and Buckles et al. (1984)[3] found the existence of the separated region of water flow near the surface of the solid waves with the height-to-length ratios $H/L = 0.125 \sim 0.2$. This fact suggests that the phase shift of the first mode of the pressure distribution in our previous study is due to the separation of the turbulent air flow near the wave surface.

In order to clarify the structure of turbulent air flow over the wave surface, including the separation of the turbulent air flow, we have measured the wind velocity over the sinusoidal wave with height-to-length ratio $H/L = 0.1$, which has been used in the previous study. The properties of the air flow studied mainly in the present paper include the vertical profiles of the mean wind speed, intensities of turbulence, turbulent Reynolds stress, and the wave induced Reynolds stress. Special attention is focused on the vertical profiles of the various quantities at each phase of the wave surface and the mean profiles averaged over one-wavelength.

2. The experiment

2.1 Preliminary experiment —measurement of the wind over a flat surface—

The experiment is carried out in a wind wave channel, 0.8 m high, 0.6 m wide and 14.6 m long. In a preliminary study, a smooth flat plate is installed horizontally near the inlet of the wind wave channel as shown in Fig. 1, and the wind over the flat plate is measured in order to obtain the reference data of the air flow field in our channel.

The total system of the measurement of the wind velocity is shown in Fig. 2. A pitot-static tube is used to measure mean velocity profiles, and it is also used to calibrate a hot wire. The Pitot-static tube is connected to the differencial pressure transducer (SOKKEN P90DL) which has sensitivity 7 mm aqFS. The

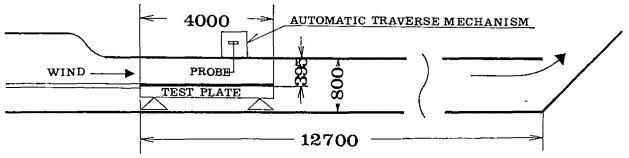

Figure 1 Schematic diagram of the wind wave channel and the test section (Unit in mm).

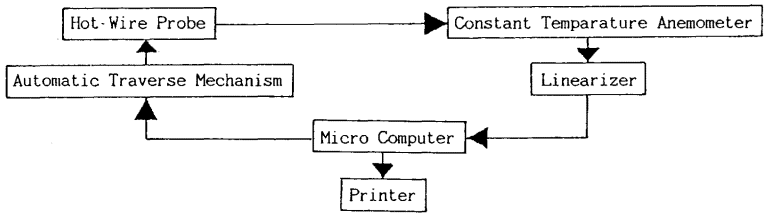

Figure 2 Total system of the measurement of wind velocity.

horizontal and vertical velocities of the turbulent air flow are measured with the hot-wire system composed of a X-probe, a constant temparature anemometer (Kanomax 1011) and a linearizer (Kanomax 1020). Alignment of the hot-wire probe in the channel is done by using a cathetometer. The output of the hot wire anemometer is sampled with sampling frequecy of 1 kHz and sampling duration of 80 sec and recorded on the F M data recorder (TEAC R-280). The Pitot-static tube and the hot-wire probe are traversed automatically and remotely by means of an automatic traverse mechanism which is controlled through a micro-computer (TEAC PS9000 MODEL216). The accuracy of its horizontal and vertical displacements is 0.2 mm. The vertical distribution of the wind is measured at the centre of the cross section of the channel, the distance of which is $X_p = 2.85$ m from the wind inlet.

The preliminaly experiment is carried out under the reference wind velocity $U_0 = 2.94$, 3.92, 5.90, 7.79(m/s), where U_0 is the maximum wind velocity at the measuring section, and its velocity corresponds roughly to the free stream velocity of the wind. Before and after the measurements of the wind, the hot-wire is calibrated by using the Pitot-static tube. Vertical profiles of the mean velocity, the turbulent intensities and the turbulent Reynolds stress will be compared with those obtained by Klebanoff (1954)[4].

2.2 Measurements of the wind over a solid wave surface

The turbulent structure over the solid wave surface is measured by replacing the flat plate with a solid wave model of twenty successive sinusoidal waves having a wavelength L of 20 cm and a wave hight H of 2 cm. A reference wind

speed $U_0 = 3.0$ m/s is used for the measurement. The Reynolds number in the present experiment is $U_0H/\nu \fallingdotseq 4000$, where U_0 is the free stream velocity above the wave, H the wave height, and ν the kinematic viscosity of the air. The turbulent air flow over the wave surface is measured with the same measuring system which has been used for the measurements of the wind over the flat plate. The vertical distribution of the wind velocity is measured at eleven sections with 2 cm separation distance starting from the windward trough to the leeward trough of the 13-th wave. Their distance from the leading edge of the wavy wall are $X_p = 2.80 \sim 3.00$ m.

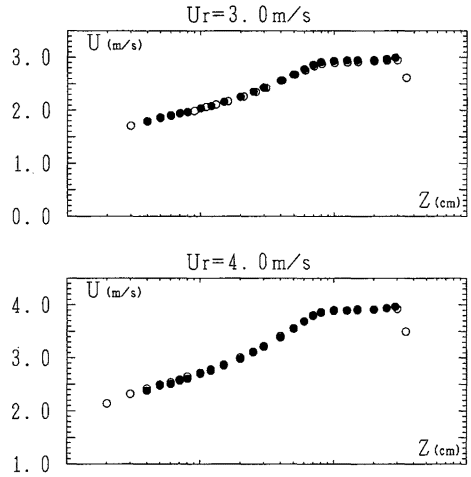

Figure 3 Mean velocity profiles over the smooth and flat plate. ○, the profile measured with hot-wire system; ●, the profile measured with a Pitot-static tube.

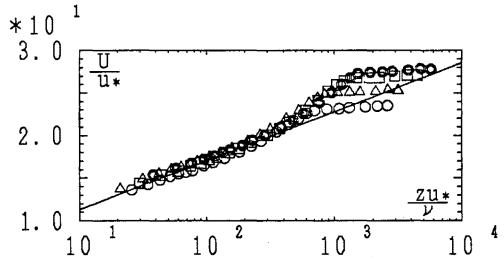

Figure 4 Mean wind profiles normalized in a standard form. ○, $Re_\delta = 1.9\times10^4$; △, $Re_\delta = 2.3\times10^4$; □, $Re_\delta = 3.5\times10^4$; ◎, $Re_\delta = 4.3\times10^4$; —, $u/u_* = 2.5 \ln(zu_*/\nu)+5.5$.
(Re_δ is the Reynolds number based on the mean velocity of free stream, U_0 and the thickness of the boundary layer, δ and kinematic viscosity of the air, ν. The friction velocity u_* is obtained by the profile method.)

3. Experimental results

3.1 Air flow over smooth and flat surface

The mean velocity profile

Figure 3 shows the mean velocity profiles over the flat plate, which have been measured respectively with the hot-wire system and with the Pitot-static tube. Agreement between both profiles is very good.

Figure 4 shows the mean wind profiles normalized in a standard form. The

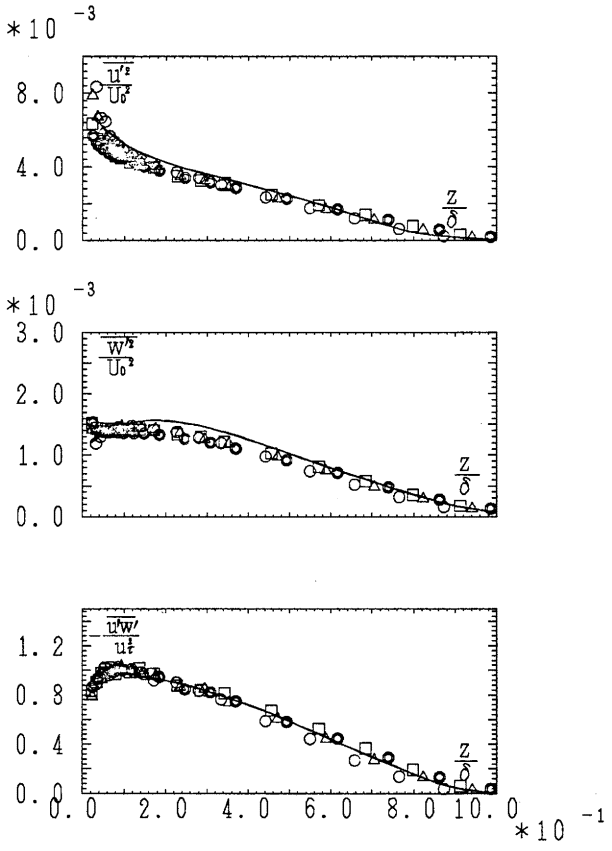

Figure 5 Vertical distributions of the turbulent intensities normalized by the free stream velocity, $\overline{u'^2}/U_\delta^2$, $\overline{w'^2}/U_\delta^2$, and the turbulent Reynolds stress nomalized by the friction velocity, $-\overline{u'w'}/u_\tau^2$. ○, $Re_\delta = 1.9\times10^4$; △, $Re_\delta = 2.3\times10^4$; □, $Re_\delta = 3.5\times10^4$; ◎, $Re_\delta = 4.3\times10^4$; —, the data of Klebanoff (1954) for $Re_\delta(= U_0\delta/\nu) = 8\times10^4$.

solid line represents a standard formla of the wind profile over the smooth flat plate

$$\frac{u}{u_*} = \frac{1}{\kappa} \ln\left(\frac{u_* z}{\nu}\right) + C \ , \tag{1}$$

where κ is von Kármán's constant ($=0.4$), u_* the friction velocity obtained by the profile method and C the constant ($=5.5$). It can be seen that the wind profile over the flat plate in our wind tunnel agree well to the standard profile.

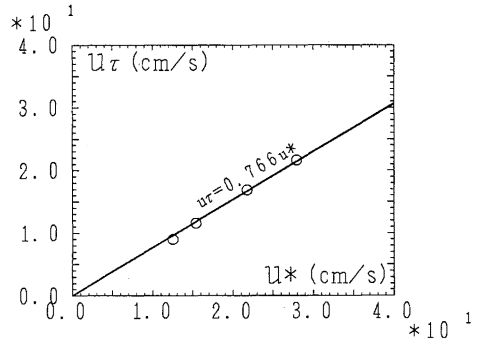

Figure 6 Comparison of the friction velocity obtained from the profile method, u_* with that obtained from the tubulent Reynolds stress in the constant stress layer, u_τ.

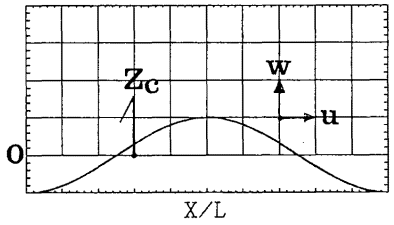

(a) Cartesian Coordinate

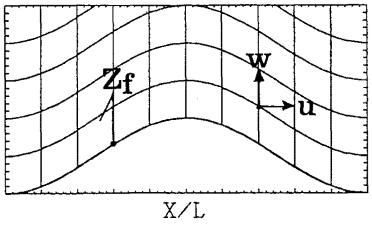

(b) Wave Following Coordinate

Figure 7 Coordinate systems.

The structure of the turbulent air flow

Figure 5 shows the vertical distribution of the turbulent intensities normalized by the free stream velocity U_0 and the turbulent Reynolds stress normalized by the friction velocity u_τ obtained from the value of $\sqrt{-\overline{u'w'}}$ in the constant stress layer. The solid curve in Fig. 5 represents the data of Klebanoff (1954)[4], which has been measured over a smooth flat plate with zero pressure gradient in the Reynolds number of $Re_\delta(=U_0\delta/\nu)=8\times10^4$. As can be seen from the figures, the present data agree well to the Klebanoff's data.

Figure 6 shows the comparison of the friction velocity obtained from the profile method, u_* with that obtained from the tubulent Reynolds stress in the constant stress layer, u_τ. The former friction velocity is about 25% larger than the latter one. We have examined the reason for this difference, but we have not obtained the definite conclusion. It should be noted, however, that the similar disagreements between the friction velocities measured with two different methods have been reported by many authors (Takeuchi et al. (1977)[5], Chen (1981)[6], Papadimitrakis et al. (1984)[7]). This must be one of the important problems to be clarified in future studies.

3.2 Air flow over the wave surface

Coordinate systems and notations of measuring quantities

Two coordinate systems shown in Fig. 7 are used in analysing the air flow over the wave surface. One is the Cartesian coordinate system (x, z_c); origin of the vertical coordinate $z_c=0$ is taken at the mean level of the wave surface. Another one is the wave following coordinate system (x, z_f) which is defined as

$$\begin{cases} x = x \\ z_f = z_c - \eta \qquad (\eta = -a\cos kx) \end{cases} \tag{2}$$

The latter coordinate system is mainly used for analyzing the air flow near the wave surface. Original data of the air flow over the wave surface is taken in the wave following coordinate system, and they are transformed into those in the Cartesian coordinate when it is needed.

Various quantities A of the air flow over the wave surface, e. g., u, w, etc., are represented as

$A(x, z, t)=\langle A\rangle(x, z)+A'(x, z, t)=\bar{A}(z)+\tilde{A}(x, z)+A'(x, z, t)$,

Here, $\langle A\rangle(x, z)$ is the time-averaged quantity defined by

$$\langle A\rangle(x, z)=\frac{1}{T}\int_0^T A(x, z, t)dt,$$

where T is the measuring time.

$\bar{A}(z)$ is x-average of $\langle A\rangle$, which is defined by

$\bar{A}(z) = \frac{1}{L}\int_0^L \langle A\rangle(x, z)dx,$
where L is the wavelength.
$\tilde{A}(x, z)$ is the wave induced perturbation defined by
$\tilde{A}(x, z) = \langle A\rangle(x, z) - \bar{A}(z)$, and
$A'(x, z, t)$ is the turbulent fluctuation defined by
$A'(x, z, t) = A(x, z, t) - \langle A\rangle(x, z)$.

Vertical profile of the wind velocity

Figure 8 shows the vertical profiles of the horizontal velocities averaged per one wavelength both in the Cartesian coordinate and in the wave following coordinate. As can be seen from Fig. 8, the two profiles agree well in the region $kz_f > 1.0 (z_f > 3.0$ cm). It seems that the wind profiles over the wave surface

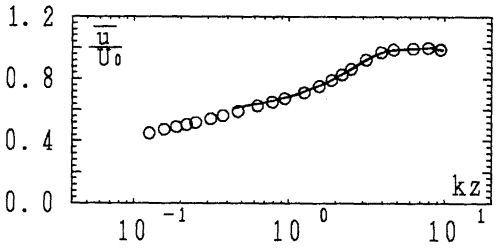

Figure 8 Comparison of the vertical distribution of the horizontal velocity averaged over one-wavelength in the Cartesian coordinate with that in the wave following coordinate. —, the profile in the Cartesian coordinate system; ○, the profile in the wave-following coorinate system.

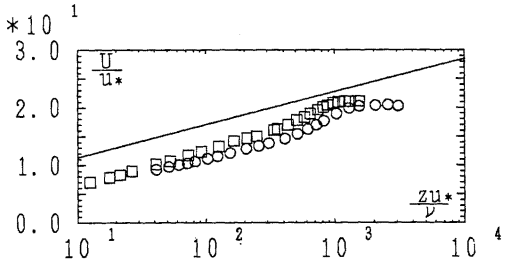

Figure 9 Comparison of the wind profile averaged over one-wavelength of the present data with that of the Kendall's data. ○, present data; □, Kendall's data; —, standatd formula for the wind profile over the smooth flat plate.
(Note: the friction volocity u_* is obtained from the profile method.)

show the logarithmic one similar to those over the flat plate.

Figure 9 shows the comparison of the present profile with the Kendall (1970)[8] 's data and with the standard formula for the wind profile over the smooth flat plate. The present profile is nearly equal to Kendall's one, though the slopes of the sinusoidal waves are different ; $ak = 0.196$ in Kendall's study and $ak = 0.314$ in our present study. Owing to the increase of the roughness parameter of the surface, the wind profiles over wave surfaces deviate from that over the smooth and flat surface.

Table 1 shows the comparison of the roghness parameter $z_0(=zexp(-x\frac{u}{u_*}))$ and the friction coefficient $C_f(=2.0(u_*/U_0)^2)$ of the wave surface with those of the flat plate, where the friction velocity u_* is determined from the profile method.

Table 1 Comparison of the roughness parameter z_0, the friction velocity obtained from the profile method u_* and the wall friction coefficient $C_f(=2.0(u_*/U_0)^2)$ of the flat plate with those of the sinusoidal plate at the same Reynolds number $Re_{xp}(=U_0X_P/\nu) \fallingdotseq 6 \times 10^5$.

Wall	U_0(cm/s)	z_0(cm)	u_*(cm/s)	C_f
Flat	295	1.50×10^{-3}	12.52	3.6×10^{-3}
Sine	302	1.19×10^{-2}	14.70	4.8×10^{-3}

Figure 10 shows the wind profile at each phase of the wave surface in the wave following coordinate, where a solid line indicates the vertical wind profile averaged over one-wavelength. In the region $kz_f < 1.0$, the wind profile changes with the phase of the waves, while in the region $kz_f > 1.0$, it does not change with the phase. The change of the wind profiles near the wave surface will be discussed later.

The structure of turbulence over wave surface

Figure 11 shows the vertical distributions of the turbulent intensities $\overline{u'^2}$, $\overline{w'^2}$ and the Reynolds stress $-\overline{u'w'}$ in the two coordinate systems, where the continuous curve shows the distributions in the fixed Cartesian coordinate and the other symbols are the distributions in the wave-following coordinate. The difference between the two profiles is small in a region $kz_f > 1.0(z_f > 3.0$ cm). This property is similar to that of the mean velocity profiles shown in Fig. 8. As can be seen from the vertical profile of the Reynolds stress $-\overline{u'w'}$, the constant stress layer exists in the region of $kz_f = 0.3 \sim 1.5$; the region corresponds to the logarithmic layer in the mean velocity profile shown in Fig. 8.

Figure 12 shows the comparison of the vertical distributions of the turbulent intensities $\overline{u'^2}$, $\overline{w'^2}$ and the turbulent Reynolds stress $-\overline{u'w'}$ for the wave surface with those for the flat surface at the same Reynolds number $Re_{XP}(=$

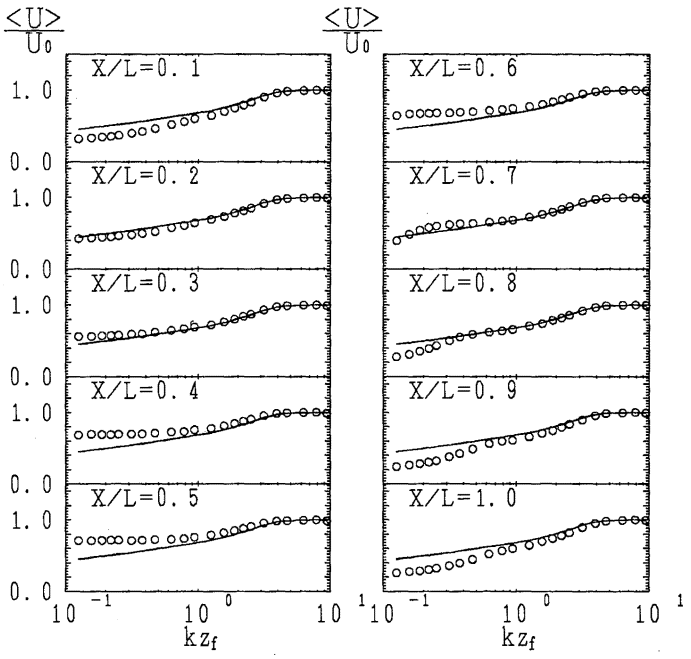

Figure 10 A series of the vertical distribution of time-averaged velocity $\langle u \rangle$ at each phase of the wave surface in the wave following coordinate: Solid line of each figure indicates the vertical wind profile averaged over one-wavelength.
(X is the longitudinal distance from the windward trough, L the wavelength of the wave surface, U_0 the mean velocity of the free stream and k the wave-numbes of the wave surface.)

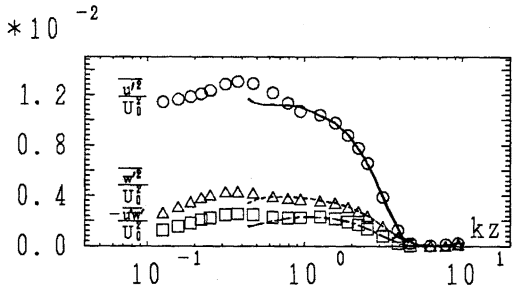

Figure 11 Comparison of the vertical distribution of the turbulent intensities $\overline{u'^2}$, $\overline{w'^2}$ and the turbulent Reynolds stress $-\overline{u'w'}$ in the Cartesian coordinate with that in the wave following coordinate. —, ---, -•-, the profiles in the Cartesian coordinate system; ○, △, □, the profiles in the wave-following coorinate system.

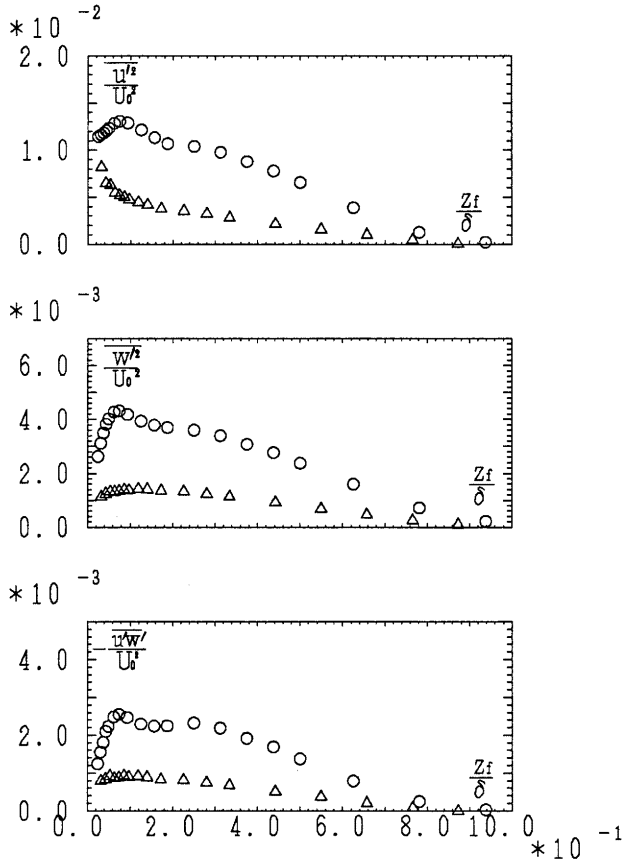

Figure 12 Comparison of the vertical distributions of the turbulent intensities $\overline{u'^2}$, $\overline{w'^2}$ and the turbulent Reynolds stress $-\overline{u'w'}$ for the wave surface with those for the flat surface at the same Reynolds number $Re_{XP}(=U_0X_P/\nu) \fallingdotseq 6\times10^5$. ○, the data for the wave surface; △, the data for the flat surface.

$U_0X_P/\nu) \fallingdotseq 6\times10^5$, where X_P is the distance from the leading edge of the test plates to the measuring station. The values of those properties for the wave surface are larger than those for the flat surface. However, if we normalized these quantities with the friction velocity u_τ, which is obtained from the Reynolds stress $\sqrt{-\overline{u'w'}}$ in the constant stress layer, the normalized intensities and the normalized turbulent Reynolds stress for the wave surface agree fairly well with those for the flat surface except for the data near the surface (Fig. 13).

Figure 14 shows the series of the verical profile of the turbulent intensity $<u'^2>$ at each phase of the wave surface in the wave following coordinate

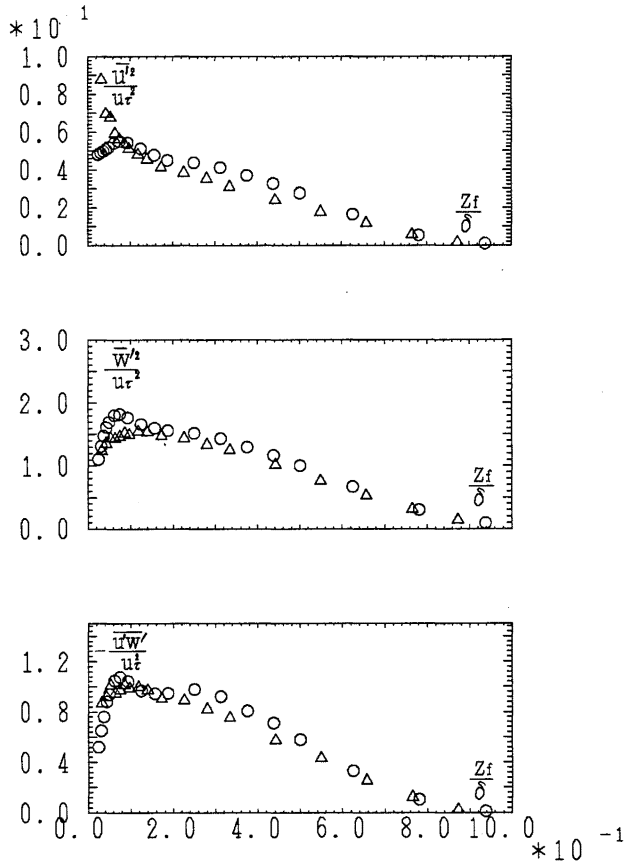

Figure 13 Comparison of the vertical distributions of the turbulent intensities $\overline{u'^2}$, $\overline{w'^2}$ and the turbulent Reynolds stress $-\overline{u'w'}$ normalized by the friction velocity u_τ for the wave surface with those for the flat surface at the same Reynolds number $Re_{XP}(= U_0X_P/\nu) \fallingdotseq 6\times10^5$. ○, the data for the wave surface; △, the data for the flat surface.

system. The profiles of windward side of the wave crest, $X/L = 0.1\sim0.5$, are not much different from the one-wavelength-averaged profile shown in the solid line, while the profiles in the leeward side of the wave crest, $X/L = 0.6\sim1.0$, show drastic change. The maximum value of the turbulent intensities near the wave surface appears at the phase of $X/L = 0.7$, and it moves upward level with the increase of the phase of X/L. The similar trend has been also observed in the vertical profile of the turbulent intensities $<w'^2>$. Such property of turbulence near the wave surface was pointed out by Buckles et al. (1979)[3]. These facts suggest that the turbulent mixing region exists at the leeward side of the wave crest.

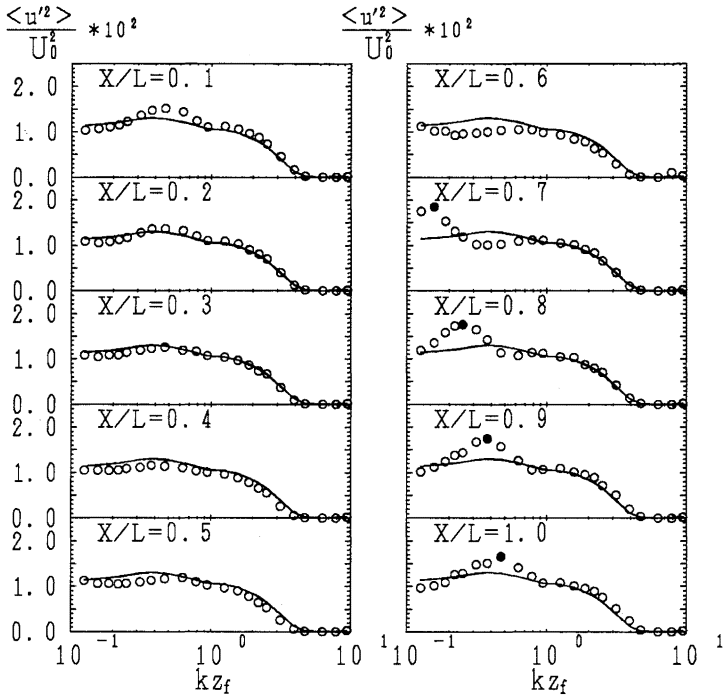

Figure 14 A series of the verical distributions of the turbulent intensity $\langle u'^2\rangle$ at each phase of the wave surface in the wave following coordinate system. The solid symbol indicates the maximum value of the turbulent intensity.

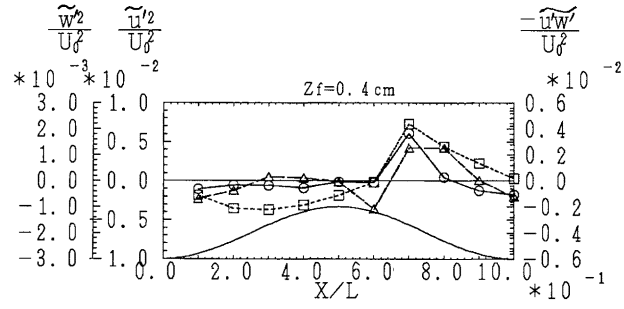

Figure 15 Longitudinal distributions of the turbulent intensities and the turbulent Reynolds stress at the height of $z_f = 0.4$ cm. ○, $(\langle u'^2\rangle - \overline{u'^2})/U_0^2$; △, $(\langle w'^2\rangle - \overline{w'^2})/U_0^2$; □, $(\langle -u'w'\rangle + \overline{u'w'})/U_0^2$.
(Note that the wind blows from the left to the right.)

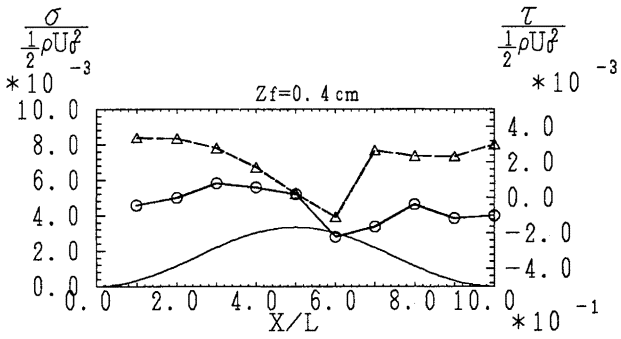

Figure 16 Longitudinal distributions of the turbulent normal stress σ and the turbulent tangential stress τ along the constant height $z_f = 0.4$ cm. ○, $\sigma/\frac{1}{2}\rho U_0$; △, $\tau/\frac{1}{2}\rho U_0$.

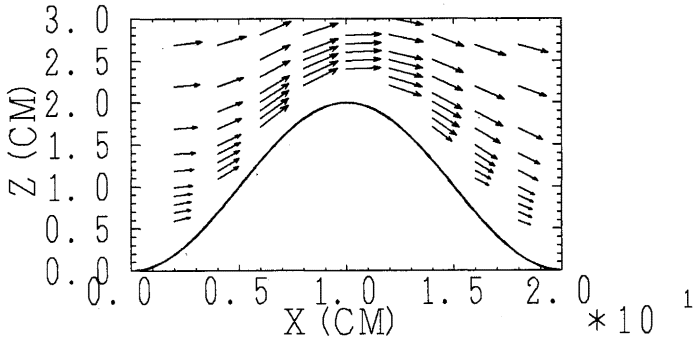

Figure 17 Flow pattern near the wave surface. The length of the arrow is proportional to the wind speed.

Figure 15 shows the longitudinal distribution of the intensities of the turbulence and the turbulent Reynolds stress along the height of $z_f = 0.4$ cm. The drastic increase of the intensities of the turbulence and the turbulent Reynolds stress can be seen at $X/L = 0.7$. In order to clarify the phenomena of the leeward side of the wave crest more in detail, the normal stress σ and the shear stress τ of the turbulence acting on the local tangential plane of the wave surface are calculated as

$$\begin{cases} \sigma = \tau_{xx}\sin^2\theta + \tau_{zz}\cos^2\theta + \tau_{xz}\sin 2\theta \\ \tau = (\tau_{xx} - \tau_{zz})\sin\theta\cos\theta + \tau_{zz}\cos 2\theta \\ \tau_{xx} = \rho\overline{u'^2}\ , \quad \tau_{zz} = \rho\overline{w'^2}\ , \quad \tau_{xz} = -\rho\overline{u'w'} + \mu\dfrac{du}{dz}\ , \end{cases} \tag{3}$$

where μ is the viscosity of the air and θ the angle between the local tangential plane of the wave surface and the horizontal plane. The longitudinal distributions of σ and τ along the wave surface are shown in Fig. 16. The values of σ and τ gradually decrease with the increase of X/L, until they have the minimum values at the leeward side of the wave crest $X/L = 0.6$. In particular, the tangential stress τ takes the minus value near the phase $X/L = 0.6$. Then the values of σ and τ drastically increase in a region between $X/L = 0.6$ and $X/L = 0.8$. These facts suggest that the air flow separates from the wave crest and reattaches at its leeward side. The similar phenomena has been also found by Zilker & Hanratty (1979)[2] and by Buckles et al. (1984)[3] in their experiments where the turbulent water flow along the sinusoidal waves with the wave height-to-length ratio $H/L = 0.12 \sim 0.2$ have been investigated.

Wave-induced fluctuations of the air flow

Figure 17 shows the flow pattern near the wave surface. It can be seen that the air flows roughly along the wave surface. In order to investigate the effect of the wave surface on the mean wind velocity more in detail, we analyze the Fourier components of the wave induced velocity fluctuations $\tilde{u}$ and $\tilde{w}$, namely

$$\tilde{u}(x) = \sum_{i=1}^{n} a_{ui}(z) \cos(k_i x - \theta_{ui}), \quad \tilde{w}(x) = \sum_{i=1}^{n} a_{wi}(z) \cos(k_i x - \theta_{wi}), \qquad (4)$$

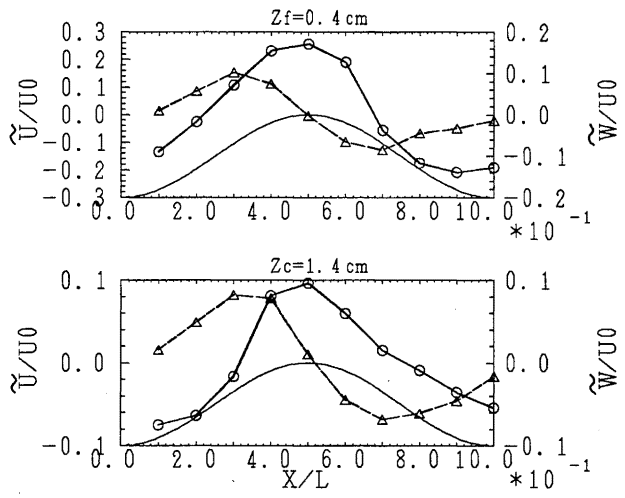

Figure 18 Longitudinal distributions of the wave induced velocity fluctuations $\tilde{u}$ and $\tilde{w}$ at the height $z_c = 1.4$ cm in the Cartesian coordinate (below) and that at the height $z_f = 0.4$ cm in the wave following coodinate (above). ○, $\tilde{u}/U_0$; △, $\tilde{w}/U_0$.

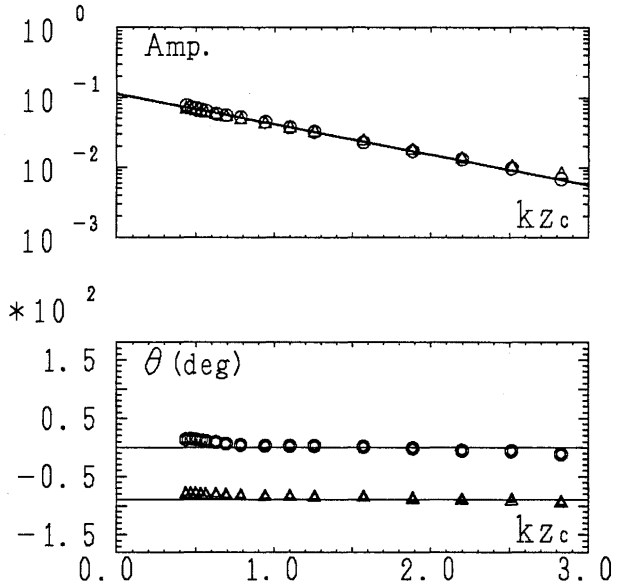

Figure 19 Vertical profiles of the first Fourier components of the wave induced velocities $\tilde{u}$ and $\tilde{w}$ in the Cartesian coordinate. ○, α_{u1}/U_0; △, α_{w1}/U_0; ◎, θ_{u1}; ▲, θ_{w1}.

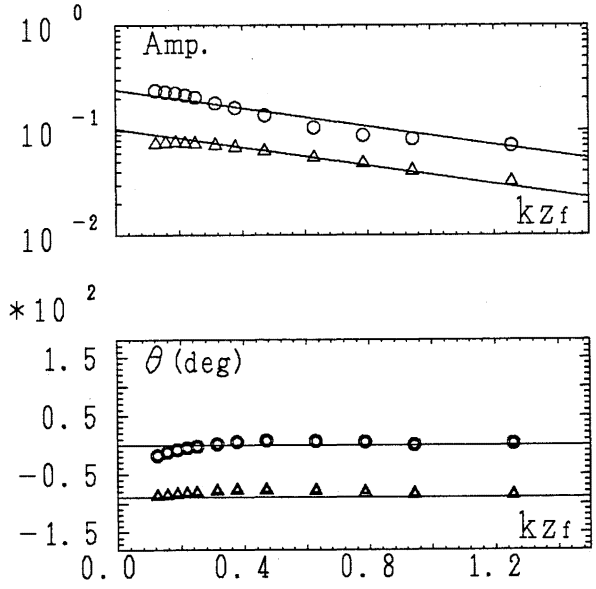

Figure 20 Vertical profiles of the first Fourier components of the wave induced velocity $\tilde{u}$ and $\tilde{w}$ in the wave-following coordinate. ○, α_{u1}/U_0; △, α_{w1}/U_0; ◎, θ_{u1}; ▲, θ_{w1}.

where a_{ui} and θ_{ui} are the amplitude and the phase of the i-th component of wave induced horizontal velocity fluctuation $\tilde{u}$, and a_{wi} and θ_{wi} are those of wave induced vertical velocity fluctuation $\tilde{w}$.

Figure 18 shows the longitudinal distributions of the wave induced velocity

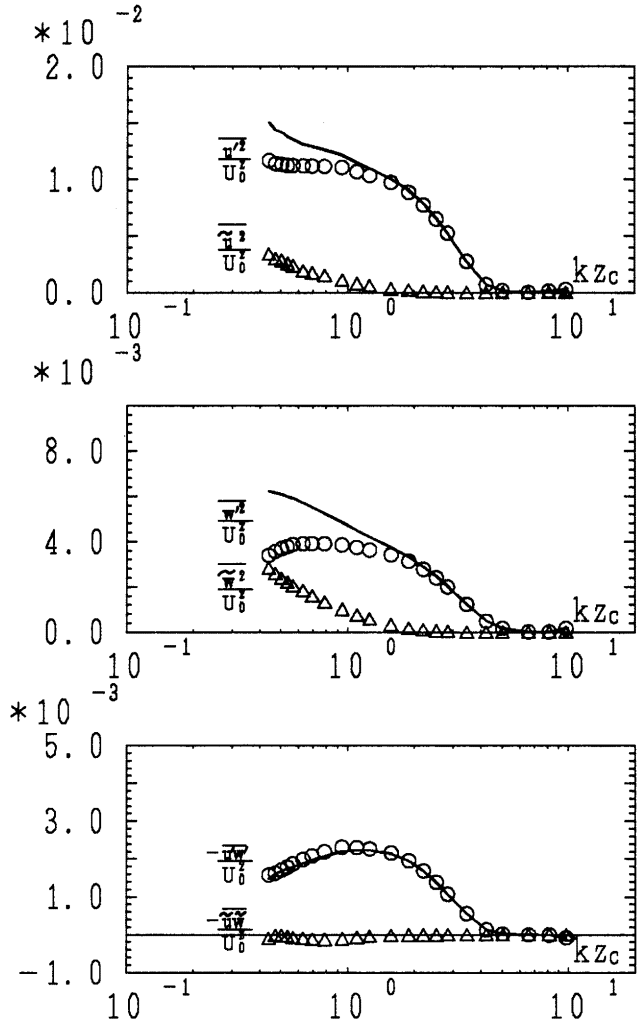

Figure 21 Comparison of the vertical distributions of the intensities of the wave induced fluctuations, $\overline{\tilde{u}^2}$, $\overline{\tilde{w}^2}$ and the wave induced Reynolds stress, $-\overline{\tilde{u}\tilde{w}}$, with those of the intensities of the turbulence, $\overline{u'^2}$, $\overline{w'^2}$, and the turbulent Reynolds stress, $-\overline{u'w'}$. ○, the data for the turbulent properties: △, the data for the wave induced properties; —, the data for the summation of the two.

fluctuations $\tilde{u}$ and $\tilde{w}$ both in the Cartesian coordinate and in the wave following coodinate. As seen in this figure, the distributions of the wave induced velocities in the Cartesian coordinate are slightly different from the sinusoidal form. The amplitudes of the higher harmonics of $\tilde{u}$ and $\tilde{w}$ are about 20~30% of those of first components. On the other hand, the wave induced velocity fluctuations in the wave following coordinate show the sinusoidal forms and their higher harmonics are less than a few percent of the first components. Therefore the wave induced velocities $\tilde{u}$ and $\tilde{w}$ do not show the linear response to the wave suface if Cartesian coodinate system is used.

The vertical profiles of the first Fourier components of the wave induced velocity $\tilde{u}$ and $\tilde{w}$ in the Cartesian coordinate are shown in Fig. 19. The amplitudes normalized with U_0, i. e. a_{u1}/U_0 and a_{w1}/U_0, show nearly exponential decay with the increase of height, and the magnitude of a_{u1}/U_0 is nearly equal to that of a_{w1}/U_0. The phase of the velocity fluctuations of the first components, θ_{u1} and θ_{w1}, follow approximately to the potential theory except in the region very close to the wave surface.

Figure 20 shows the Fourier components of the wave-induced velocity fluctuations analyzed in the wave following coordinate. Phase shift can be clearly seen near the wave surface. This may be attributed to the existence of the turbulent mixing region caused by the air flow separation discussed previously.

Figure 21 shows the comparison of the vertical distributions of the intensitites of the wave-induced fluctuations, $\overline{\tilde{u}^2}$, $\overline{\tilde{w}^2}$ and wave-induced Reynolds stress, $-\overline{\tilde{u}\tilde{w}}$, with those of the intensities of the turbulence, $\overline{u'^2}$, $\overline{w'^2}$ and the turbulent Reynolds stress, $-\overline{u'w'}$. The wave-induced intensities and the wave induced Reynolds stress are smaller than the turbulent intensities and the turbulent Reynolds stress except for the wave induced intensity $\overline{\tilde{w}^2}$ near the wave surface.

Downward flux of the wind momentum

The downward flux of the wind momentum per one wavelength is obtained from three methods. First one is so called the profile method. In this method, the momentum flux M_{X1} is estimated from the friction velicity u_* obtained by applying the logarithmic distribution to the mean velocity profile as

$$M_{x1} = \rho u_*^2 \ . \tag{5}$$

Second one is the direct measurement of the downward flux of the wind momentum in the constant stress layer as

$$M_{X2} = -\rho(\bar{u}\bar{w} + \overline{u'w'} + \overline{\tilde{u}\tilde{w}})$$

Since $\bar{w}$ is assumed to be zero, above equation reduced to

$$M_{x2} = -\rho(\overline{u'w'} + \overline{\tilde{u}\tilde{w}}) \ .$$

The vertical profiles of the turbulent Reynolds stress $-\overline{u'w'}$ and the wave-induced Reynolds stress $-\overline{\tilde{u}\tilde{w}}$ are shown in Fig. 21. As shown in this figure, the wave-induced Reynolds stress, $-\overline{\tilde{u}\tilde{w}}$ is negligible as compared to the turbulent Reynolds stress $-\overline{u'w'}$. Therefore M_{X2} is approximated by

$$M_{X2} = -\overline{\rho u'w'} \ . \tag{6}$$

Third method is the direct measurements of the pressure P and the shear stress τ_0 along the wave surface, namely

$$M_{X3} = \overline{P\frac{\partial\eta}{\partial x}} + \overline{\tau_0} \tag{7}$$

In the present study, however, since we have not measured τ_0 along the wave surface, we estimated $\overline{\tau_0}$ as

$$\overline{\tau_0} = \overline{\sigma\frac{\partial\eta}{\partial x}} + \overline{\tau} \tag{8}$$

where σ and τ are the turbulent normal stress and tangential stress acting on the local tangential plane of the wave-following line, which have been estimated from the turbulence measured at the height of $z_f = 0.4$ cm. The ratio of the

Table 2 Downward flux of the wind moment normalized with $\frac{1}{2}\rho U_0^2$. (Note: $Cd_1 = 2.0(u_*/U_0)^2$, $Cd_2 = -2.0\overline{u'w'}/U_0^2$, $Cd_3 = \left(\overline{P\frac{\partial\eta}{\partial x}} + \overline{\sigma\frac{\partial\eta}{\partial x}} + \overline{\tau}\right)\Big/\frac{1}{2}\rho U_0^2$.)

Cd_1	Cd_2	$\overline{P\frac{\partial\eta}{\partial x}}/\frac{1}{2}\rho U_0^2$	$\overline{\sigma\frac{\partial\eta}{\partial x}}/\frac{1}{2}\rho U_0^2$	$\overline{\tau}$	Cd_3
4.8×10^{-3}	4.4×10^{-3}	6.1×10^{-3}	1.5×10^{-4}	2.1×10^{-3}	8.3×10^{-3}

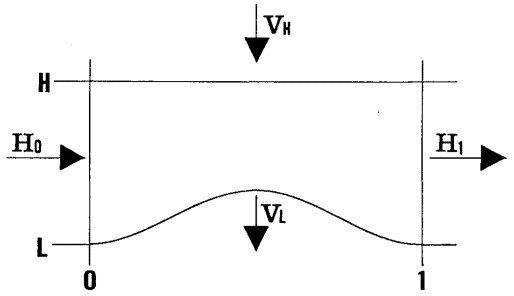

Figure 22 Budget of the momentum flux in the controll volume between any level of the logarithmic layer and the wave surface. $\left(H_0 = \int_0^{z_H}(P + \rho\langle uu\rangle)dz$ at the $X/L = 0$, $H_1 = \int_0^{z_H}(P+\rho\langle uu\rangle)dz$ at the $X/L = 1$, $V_H = M_{x2}L$ at any level of the logarithmic layer, $V_L = M_{x3}L$ along the wave surface$\right)$.

pressure contribution $\overline{P\frac{\partial\eta}{\partial x}}$ to the M_{X3} is about 70% due to the asymmetric distribution of the static pressure which is caused by the air flow separation. This ratio is considered to be dependent on the wave slope if we refer to the results of Buckles et al. (1984)[3]. The momentum fluxes calculated from above three methods are given in Table 2, where the momentum fluxes are normalized with $\frac{1}{2}\rho U_0^2$. It is shown that Cd_2 is nearly equal to Cd_1 but about half of Cd_3.

Finally we investigated the momentum budget in the controll volume between the wave surface and any level in logarithmic layer, which is shown in Fig. 22.

Curiously, the budget has shown the minus value, though the accuracy of the measurement of $\Delta\int(P+\rho\langle uu\rangle)dz$ is not as good as the other terms. The Kendall (1970)'s data has also shown the difference between $\overline{P\frac{\partial\eta}{\partial x}}\Big/\frac{1}{2}\rho U_0^2$ and Cd_1 in the data for low Reynolds number. These results suggest the existence of another contribution to the momentum balance, for example $-\rho\bar{u}\bar{w}$, though it is not investigated in the present study.

4. Conclusions

The structure of tubulent air flow over the sinusoidal wave with the wave height-to-length ratio $H/L = 0.1$ has been studied under relatively low Reynolds number $U_0H/\nu \fallingdotseq 4000$. As a preliminary study, turbulent air flow over a flat plate has been also studied in the same facilities. The following conclusions can be drawn from the present study ; In the preliminary study over the flat plate, it is confirmed that the wind profiles follows the standard logarithmic formula and the turbulent intensities and the turbulent Reynolds stress agree well to those measured by Klebanoff (1954)[4]. However, the friction velocity obtained from the profile method is about 25% larger than that obtained from the direct measurement of the turbulent Reynolds stress, though the reason for it is not clear. The experimental result over the sinusoidal wave surface is as follows.

(i) The mean velocity profile averaged over one wavelength shows the logarithmic profile. However, it did not follow the standard formula for smooth flat plate, i. e., $\frac{u}{u_*}=\frac{1}{\kappa}\ln(\frac{zu_*}{\nu})+5.5$ because the solid waves increase the roghness parameter of the surface.

(ii) The values of the turbulent intensities $\overline{u'^2}$, $\overline{w'^2}$ and the turbulent Reynolds stress $-\overline{u'w'}$ for the wave surface are larger than those for the flat plate at the same Reynolds number $Re_{XP} \fallingdotseq 6\times10^5$. However, if we normalize those parameters with the friction velocity u_τ which is obtained from the Reynolds stress $\sqrt{-\overline{u'w'}}$ in the constant stress layer, the parameters for the wave surface agree with those for the flat plate.

(iii) Negative value of the turbulent Reynolds stress τ has been observed in the leeward side of the wave crest. This fact indicates the separation of the air flow near the wave crest.

(iv) Spatial change of the wave induced velocity fluctuations in the wave following coordinate can be approximated by the first Fourier component of the same wave number with that of the wave surface. In a general sence, the phase of the wave induced velocity is nearly equal to that estimated from the potential theory, but the phase near the wave surface deviates from that estimated from the potential theory. We may say that this fact is also attributed to the air flow separation near the wave surface.

(v) The downward flux of the horizontal momentum of the air flow over the wave surface, M_X, has been determined by means of three methods; (1) The profile method based on the logarithmic profile, $M_{X1} = \rho u_*^2$, (2) The direct measurement of the turbulent Reynolds stress in the logarithmic layer, $M_{X2} = -\rho\overline{u'w'}$, where the wave induced Reynolds stress $-\rho\overline{\tilde{u}\tilde{w}}$ has been negligible in the logarithmic layer, (3) The direct measurement of the wind stress acting on the wave surface, $M_{X3} = \overline{P\frac{\partial\eta}{\partial x}} + \overline{\tau_0}$. The momentum fluxes M_{X2} and M_{X1} have shown nearly the same values but M_{X3} has been about twice as large as the former two. This suggests another contribution to the momentum flux such as $M_{x2} = -\rho\overline{u}\overline{w}$.

(vi) The the ratio of pressure contribution $\overline{P\frac{\partial\eta}{\partial x}}$ to the M_{X3} is about 70% in our present study. However, refering to the result of Buckles et al. (1984)[3], this ratio seems to be dependent on the wave slope

Acknowledgement

The authors are indebted to Mr. K. Marubayashi and Mr. M. Ishibashi for their assistance in the laboratory experiment. They also wish to express their gratitudes to Dr. A. Masuda for his many helpful discussions. This study was suported by the Grant-in-Aide for Scientific Research, Project B no. 60460049 from the Ministry of Education Science and Culture of Japan.

References

1) Bandou, T., Mitsuyasu, H., Marubayashi, K. and Ishibashi, M.: The structure of turbulent air flow over wavy wall. Part 1. Rep. Res. Inst. Appl. Mech., Kyushu Univ. 103, (1988) 53-65.

2) Zilker, D. P. and Hanratty, T. J.: Influence of the amplitude of a solid wavy wall on a turblent flow. Part 2. Separated flows. J. Fluid. Mech. 90, (1979) 257-271.

3) Buckles, J., Hanratty, T. J. and Adrian, R. J.: Turbulent flow over large-amplitude wavy surfaces. J. Fluid. Mech. 140, (1984) 27-44.

4) Klebanoff, P. S.: Characteristics of turbulence in a boundary layer with zero pressure gradient. NACA Tech. Note No. 3178 (1954).

5) Takeuchi, K., Leavitt, E. and Chao. S. P.: Effects of water waves on the structure of

turbulent shear flow. J. Fluid. Mech. 80, (1977) 535-559.
6) Chen, F.: Experimental approach to closure modeling of turbulent shear flow over a wavy surface. Ph. D. dissertation, Civil Eng. Dept., Stanford Univ. 219, (1981).
7) Papadimitrakis, Y. A., Hsu, E. Y. and Street, R. L.: On the structure of the velocity field over progressive mechanically-generated water waves. J. Phys. Oceanogr. 14, (1984) 1937-1948.
8) Kendall, J. M.: The turbulent boundary layer over a wall with progressive surface waves. J. Fluid. Mech. 41, (1970) 259-281.

(Received July 12, 1988)